Communications in Information and Systems
Volume 22, Number 4, 459–475, 2022

# Fluorescence oxygen sensor array for non-contact and rapid measurement of oxygen consumption rate of single oocyte

Hisataka Maruyama and Fumihito Arai

Evaluation of oocytes and embryos is an important technique for many biomedical applications. In this study, we proposed a method to measure individual oocytes' oxygen consumption rate by fluorescence oxygen measurement using a fluorescent oxygen sensor arranged in a striped pattern on a microchamber. For oxygen concentration measurement, a fluorescent oxygen microsensor array was prepared using a hydrophilic photo-crosslinkable resin and fluorescent oxygen indicator. The sensor was fabricated by forming a stripe pattern on polydimethylsiloxane using photopolymerization and molding methods. Since the oxygen permeabilities of polydimethylsiloxane and the medium are similar, the oxygen concentration distribution around the oocyte follows the spherical diffusion theory. The sensor array was used to detect the distribution of oxygen concentration in two-dimensional plane. The oxygen consumption rate of the single oocyte was obtained by image analysis and Fick's law. A single mouse oocyte's oxygen consumption rate on the microchamber could be measured without contact of sensor probe to the target oocyte within 8 seconds ($0.59 \pm 0.03$ fmol/s).

## 1. Introduction

In these days, evaluation of oocyte's quality becomes an important technique in many biomedical applications and has played a major role in improvement of the breeding of animals and fertilization treatment [1, 2]. High-throughput screening of oocytes can shorten the process time and improve oocyte development rates. Evaluation of oocyte from morphological information was used owing to its noninvasive nature [3]. However, accurate morphological evaluation requires a highly skilled technician and is not quantitative. Therefore, improved methods for quantitative evaluation are required. For example, objective evaluation has been achieved using metabolic measurements. The oocyte produces adenosine triphosphate (ATP) by pyruvate oxidation using oxygen during glucose consumption and metabolism [4, 5, 6, 7, 8].

Thus, measurement of the oxygen consumption can provide a readout to represent metabolic activity. However, oxygen consumption measurement is challenging for single oocytes and is therefore not widely used. Several methods, including spectrophotometric assays [8, 9, 10], scanning electrochemical microscopy (SECM) [11, 12, 13], fluorescent measurement [14, 15, 16], have been developed to measure oxygen consumption rates (OCRs). In spectrophotometric assays, multiple oocytes are introduced to a cuvette including the solution with oxyhemoglobin. The increase of light absorbance represents the decrease of oxyhemoglobin by the decrease of oxygen inside the cuvette. This change is detected using a photometer. This measurement method is noninvasive because no chemical treatment is required for measurement of oxygen concentration. But this measurement method requires multiple oocytes, because the sensitivity of this measurement method is not enough to measure the OCR of a single oocyte. In SECM, OCR is measured from profile of the oxygen concentration around the oocyte by scanning the oxygen electrode. This method can be applied for single oocyte measurement. However, SECM method requires long time for acquiring profile of oxygen concentration because repeated tip scanning is required. Moreover, the oxygen electrode is easily broken, and the target oocyte is damaged during tip scanning. In the fluorescent measurement, the oocyte is stained with a fluorescent oxygen indicator. The oxygen concentration of the oocyte is measured from the change of fluorescence intensity caused by decreasing the oocyte's oxygen concentration. However, direct fluorescent measurement is not suitable for the biomedical applications because the stained oocyte received some effects from the fluorescent indicator and fluorescent staining requires long time. Therefore, we proposed a non-contact and rapid measurement of a single oocyte's OCR by fluorescent oxygen sensor array on a microchamber (Figure 1). The chip is consisted of polydimethylsiloxane (PDMS) and fabricated by photolithography and replica molding. The fluorescent oxygen sensor is consisted of polyethylene glycol diacrylate 575 (PEGDA 575) and $Ru(bpy)_3Cl_2$ [14]. The fluorescent oxygen sensor is constructed in a striped pattern to maintain spherical diffusion of oxygen around the oocyte on the microchamber. The single oocyte's OCR is calculated by the image analysis of fluorescent images and the spherical diffusion theory. Compared to other methods, this method has the advantage of non-contact, rapid, and measurement of the profile of oxygen concentration in two-dimensional plane. In addition, the OCR measurement can be performed in standard culture conditions using a microchamber made of biocompatible materials.

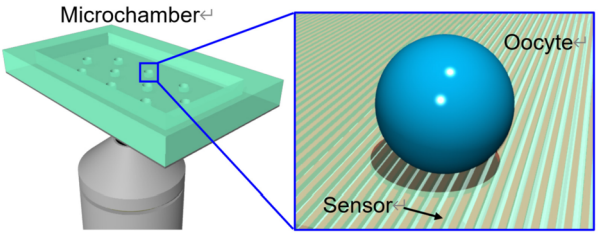


Figure 1: A schematic diagram of fluorescent measurement of the oxygen consumption rate (OCR) of single oocytes on microchamber.

## 2. Materials and methods

### 2.1. Fluorescent measurement system

The measurement system equipped for fluorescent sensing system is consisted of a commercialized microscope (Ti-E; Nikon) with an objective lens (Plan Apo 10×; magnification: 10×; Nikon) and a 16-bit EM-CCD (iXon Ultra; Andor, 512×512 pixels), and a laser confocal system (CSU-X1; Yokogawa) as shown in Figure 2 [17, 18]. 488 nm laser (Power: 20 mW) is utilized to excite fluorescent oxygen sensor. A light absorption filter that absorbs 488nm light is placed in front of the EM-CCD. A stage-top incubator (Zilcos; Tokai Hit Co., Ltd.) was utilized for the temperature control (accuracy ±0.3 K) and the $CO_2$ concentration control (5%). The stepping motor of the microscope was used to control the Z-axis. The microscope was also equipped with a perfect focus system (PFS) that maintained the focus in response to the thermal drift. The precision of the Z-axis control by PFS was 50 nm. The operator controlled the stage using a stepper motor. The fluorescent images from the sensor were acquired using an EM-CCD.

$Ru(bpy)_3Cl_2$ is the chloride salt coordination complex utilized as a fluorescent oxygen indicator. The excitation and emission wavelength of $Ru(bpy)_3Cl_2$ are 561 nm and 620 nm, respectively. Fluorescent intensity is represented by equation 1 [18].

$$I = I_0 \cdot \Phi \cdot M \cdot \epsilon \cdot l \cdot exp(-t/\tau) \tag{1}$$

where $I$ [W] is the fluorescence intensity emitted from the fluorescent material per unit time. $I_0$ [W] is the excitation light flux of the fluorescent material. $\Phi$ is the fluorescence quantum yield. $M$ [mol/L] is the concentration of the fluorescent dye. $\epsilon$ is the absorbance index [L/mol·m]. $l$ [m] is

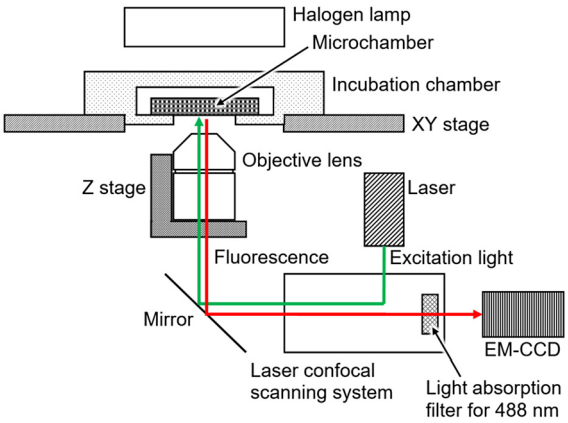


Figure 2: A schematic diagram of fluorescent measurement system.

the pass length of emitting fluorescence to EM-CCD. $t$ [s] is the total exposure time. and $\tau$ [s] is the decay coefficient of the fluorescence intensity. The fluorescence quantum yield of $Ru(bpy)_3Cl_2$ increases according to the decrease of oxygen concentration. On the other hand, the excitation light flux, fluorescent dye concentration, absorbance index, and pass length are considered constant parameters of the oxygen sensor made in the microchamber. Therefore, the change of oxygen concentration is measured from the change in fluorescence intensity of the fluorescent oxygen sensor.

### 2.2. Analytical model of OCR measurement

The proposed OCR measurement method had the following assumptions:

1) The cytoplasm must be spherical.
2) The oocyte must be filled with cytoplasm.
3) The mitochondria must be evenly distributed in the cytoplasm.
4) The zona pellucida does not affect the OCR measurement.

In stationary state, the single oocyte's OCR was calculated by the spherical diffusion theory. The analytical model for the OCR measurement is shown in Figure 3. The oocyte is placed on a PDMS microchamber with oxygen sensor array and filled with culture medium. The oxygen diffusion coefficient of the PDMS is assumed to be the same as that of the culture medium. And the oxygen sensor array is patterned not to interfere with oxygen diffusion in the PDMS. The oxygen flow rate of the oocyte $f_s$ [mol/m$^2$s] was determined by Fick's law as shown in equation 2.

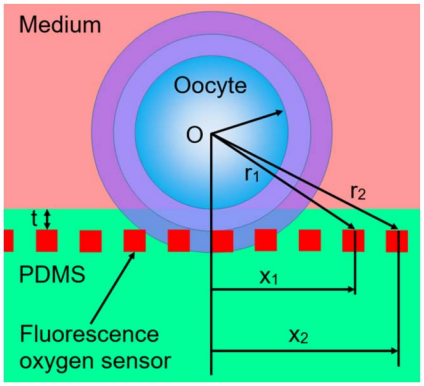


Figure 3: Analytical model of OCR measurement.

$$f_s = D\frac{dC(r)}{dr}dS \tag{2}$$

where $r$ [m] is distance from the center of the oocyte, $D$ [m] is the PDMS's oxygen diffusion coefficient ($2.18 \times 10^{-9}$ m$^2$/s at 37°C), $C(r)$ is the oxygen concentration profile [mol/L], and $S$ [m$^2$] is the oocyte's surface area. $r$ is represented by equation 3.

$$r = \sqrt{(r_s + t)^2 + x^2} \tag{3}$$

$r_s$ [m] is the oocyte's radius, $t$ [m] is the thickness of PDMS between the oocyte and the sensor, and $x$ [m] is horizontal distance from the center of the oocyte. From equations 2 and 3, the oocyte's OCR can be calculated as follows (equation 4).

$$F = f \times S = 4\pi {r_s}^2 \cdot D\frac{dC(r_s)}{dr} \tag{4}$$

In equation 4, the gradient of the oxygen concentration at $r_s$ is determined based on the profile of the oxygen concentration fitted by least squares at $r_s$. This method's advantage is that the PDMS's oxygen permeability is similar to the oxygen permeability of water. Thus, oxygen concentration around the oocyte maintains the spherical diffusion. Furthermore, this method measures oxygen concentration distribution in the two-dimensional plane by image processing of the fluorescent images, so that the distribution of the OCR of the oocyte can be obtained.

### 2.3. Diffusion analysis of oxygen concentration by finite element method

The oxygen concentration distribution around an oocyte in three-dimensional space was analyzed using finite element method (FEM) (COMSOL Multiphysics 4.4; COMSOL AB). This FEM analysis was used to determine the design of the fluorescent sensor. Table 1 shows the analytical parameters for FEM. In this study, oocytes with a diameter of 75 $\mu$m were targeted [19]. The OCR of the mouse oocyte was set to 1 fmol/s based on previous studies, and the oxygen diffusion coefficient of the medium was set to the same value as that of PDMS. The oxygen diffusion coefficient of the sensor was determined from that of PEGDA 575. The PDMS's thickness between the oocyte and the sensor was set to 10 $\mu$m.

Table 1: Parameters in FEM analysis

| Parameters | Value |
|---|---|
| Bulk oxygen concentration [$\mu$mol/m] | 0.21 |
| Diameter of oocyte [$\mu$m] | 75 |
| Oxygen consumption rate [mol/s] | $1.0 \times 10^{-15}$ |
| Oxygen diffusion coefficient (Medium) [$m^2$/s] | $2.18 \times 10^{-19}$ |
| Oxygen diffusion coefficient (PDMS) [$m^2$/s] | $2.18 \times 10^{-19}$ |
| Oxygen diffusion coefficient (Sensor) [$m^2$/s] | $3.4 \times 10^{-11}$ |

Figure 4 shows the FEM results of the pattern of fluorescent sensor. The diffusion coefficient of oxygen of PEGDA 575 was much lower than that of PDMS and culture medium. Therefore, the pattern of the fluorescent sensor should be designed so that it does not interfere with the diffusion of oxygen. From the analysis results, a stripe pattern with a pitch of 5 $\mu$m was found to be suitable for maintaining the spherical diffusion of oxygen.

Figure 5 shows the FEM results of thickness of PDMS required to apply the spherical diffusion theory to this measurement. The glass placed underneath the PDMS for stable observation was not able to transmit oxygen. Therefore, the PDMS's thickness between the oocyte and the fluorescent sensor must be designed appropriately. From the results of this analysis, we found that a thickness of more than 300 $\mu$m is necessary for oxygen measurement.

From these FEM results, the PDMS thickness of 500 $\mu$m and the stripe pattern with a 5 $\mu$m pitch for the sensor layout were determined.

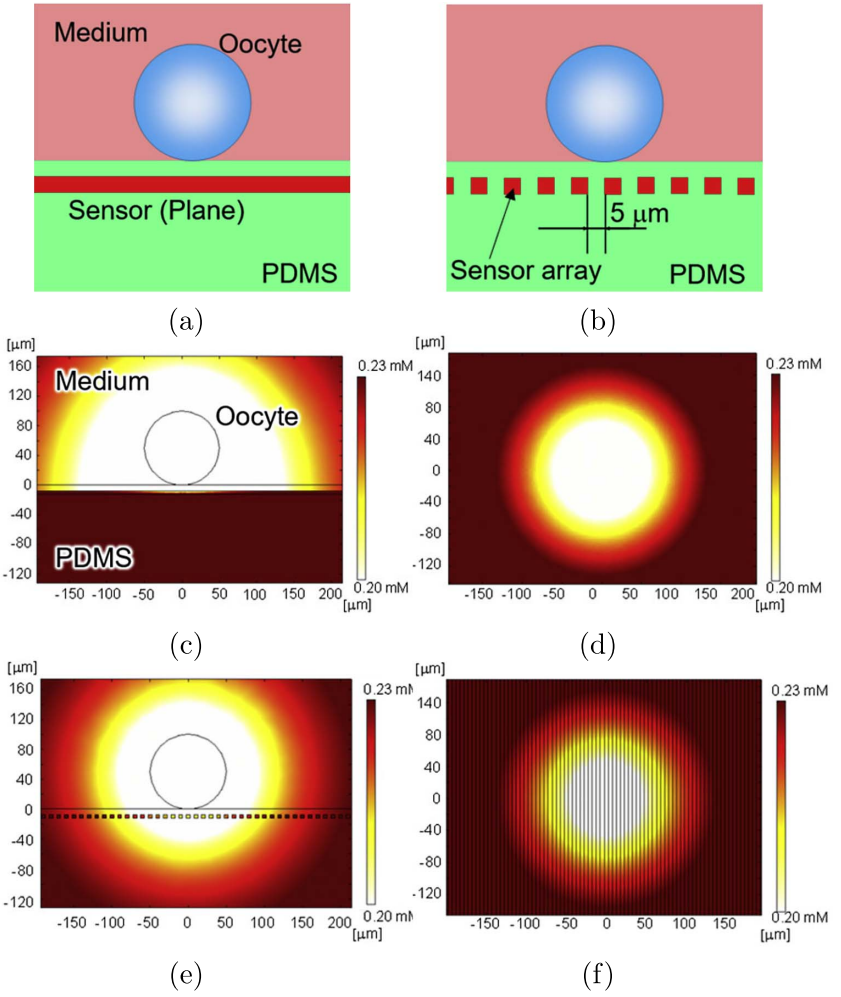


Figure 4: FEM analysis results for oxygen diffusion according to sensor layout. (a) A schematic diagram of analytical model with plane sensor. (b) A schematic diagram of analytical model with stripe sensor. (c) Result on a plate sensor pattern (Cross view). (d) Result on a plate sensor pattern (Top view). (e) Result on a striped sensor pattern with 5 $\mu$m pitch (Cross view). (f) Result on a striped sensor pattern with 5 $\mu$m pitch (Top view).

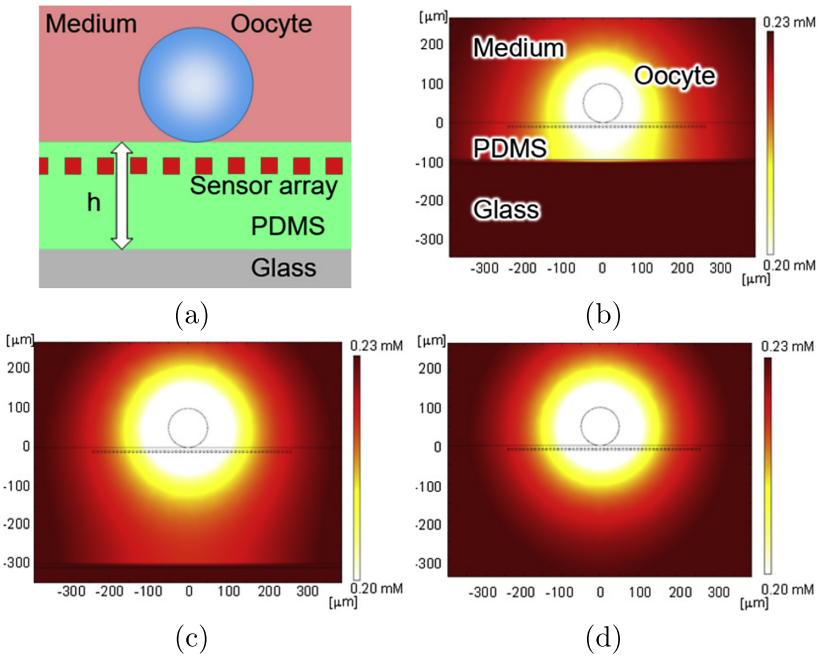


Figure 5: FEM analysis result for oxygen diffusion according to the PDMS thickness. (a) A schematic diagram of analytical model. (b) Result (PDMS thickness: h= 100$\mu$m). (c) Result (PDMS thickness: h= 300$\mu$m). (d) Result (PDMS thickness: h= 500$\mu$m).

### 2.4. Fabrication process of the microchamber and fluorescent oxygen microsensor array

Figure 6 (a)-(d) shows the fabrication process of the microchamber with the fluorescent oxygen sensor array. The microchamber is mainly consist of polydimethylsiloxane (PDMS; Sylpot 184, Dow.com). The fluorescent oxygen microsensor is consists of polyethylene glycol diacrylate 575 (PEGDA575, Sigma Aldrich) which is a hydrophilic photo-crosslinkable resin, $Ru(bpy)_3Cl_2$, and Darocure 1173 (Chiba Chemical Japan) which is a photo-initiator. Fabrication process of the microchamber having fluorescent oxygen microsensor is as follows.

1) Spin-coat negative photoresist SU-8 3005 (Kayaku Advanced Materials) on the silicon substrate at 4000 rpm for 30 s (Thickness: 5 $\mu$m).
2) Photo-pattern of the coated photoresist to stripe-shaped (width: 5 mm, Gap: 5 $\mu$m). (Figure 6 (a))

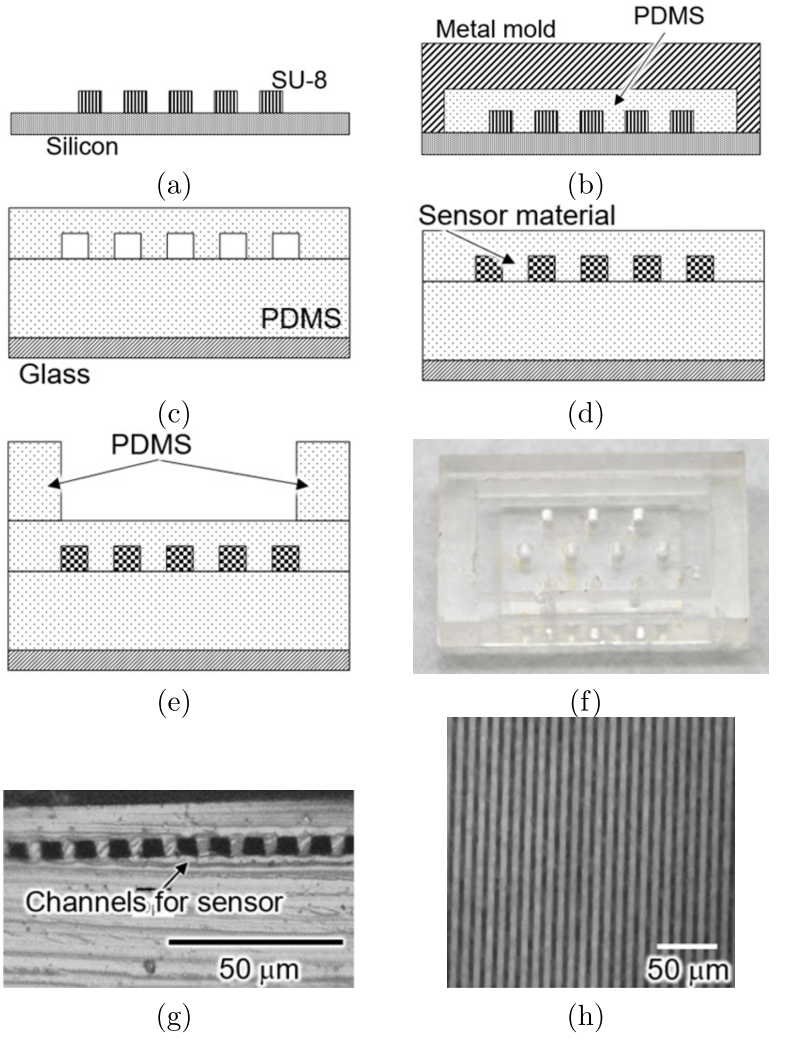


Figure 6: Fabrication process of the microchamber. (a) Fabrication of microchannel mold on silicon substrate. (b) Molding by PDMS. (c) Peel the cured PDMS microchannel and bond to the PDMS sheet (d) Injection of PEGDA 575 and photopolymerization. (e) Bond the PDMS layer with halls to the PDMS microchamber (f) Photograph of the microchamber. (g) Cross-sectional photograph of the microchamber. (h) Fluorescent image of the oxygen sensor array.

3) Put the metal jig on the silicon substrate, pour the polydimethylsiloxane (PDMS; Sylpot 184, Dow) into the gap between the metal jig and the silicon substrate, and then bake at 80°C for 1 hour. (Figure 6 (b))
4) Peel the cured PDMS and bond to the PDMS sheet (Thickness: 0.5 mm) on the glass substrate (Thickness: 0.3 mm). (Figure 6 (c))
5) Injection of the sensor material (3.5 mM $Ru(bpy)_3Cl_2$ in PEGDA575 with 5% Darocure 1173) and photopolymerization by exposure of 365 nm light by exposure unit (BOX-S3000, Sunhayato). (Figure 6 (d))
6) Bond the PDMS layer with halls of 2 mm diameter to the PDMS microchamber. (Fig. 6 (e)) As shown in Figure 6 (f), 10 microchambers were placed on one chip. Figure 6(g) and Figure 6(h) show the bright-field cross-sectional view of the PDMS substrate with the fluorescent sensor, and the fluorescent image, respectively.

## 3. Results

### 3.1. Calibration of fluorescent oxygen sensor

Figure 7(a) shows the calibration results for relative fluorescence intensity with oxygen concentration. The calibration experiment was conducted with the Ti-E and ZILCOS. The relative fluorescence intensity was then calculated concerning the saturated oxygen concentration (210 $\mu$M, 37°C). Calibration experiments have been conducted five times. Figure 7(a) plots the mean and standard deviation of fluorescence intensity at each oxygen concentration. The results showed that there was a correlation between the oxygen concentration and the relative fluorescence intensity. Using equation 5, the profile of oxygen concentration was calculated from the fluorescence image.

$$[O_2] = -8.3 \times 10^2 \cdot \frac{I}{I_0} + 1.1 \times 10^3 \tag{5}$$

In the experimental system, the fluorescent oxygen sensor had a resolution of 1.3 $\mu$mol/L for the oxygen concentration and a spatial resolution of 5 $\mu$m for the measurement from this calibration. This sensitivity of the sensor was comparable to the commercially available electrode-type oxygen sensor [20]. Figure 7(b) shows the photodegradation of the fluorescent sensor. The sensor's fluorescence intensity was maintained at almost the same intensity even after 600 s of excitation since $Ru(bpy)_3Cl_2$ represents low photodegradation (variation was about 1%). This evaluation was done three

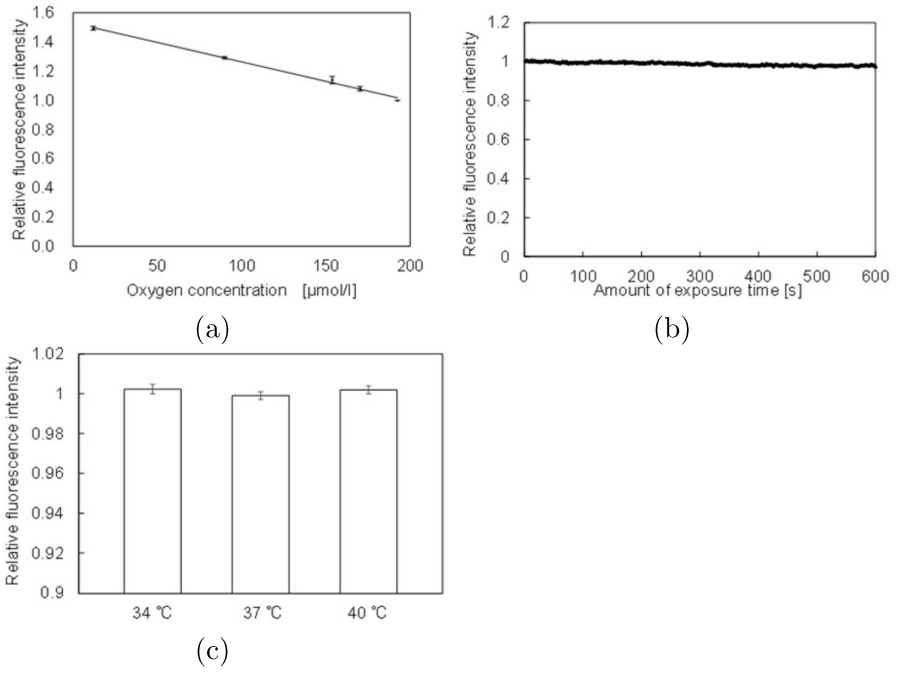


Figure 7: Evaluation of fluorescent oxygen sensor. (a) Calibration of the relative fluorescent intensity with oxygen concentrations, (b) Evaluation of photodegradation of the fluorescent oxygen sensor, (c) Evaluation of the stability of fluorescent intensity according to temperature.

times. When the fluorescence intensity change from the start of measurement to 600 seconds was fitted by the least-squares method, the slope was $-4.2 \times 10^{-4} \pm 0.4 \times 10^{-4}$ %/s. In the OCR measurement, excitation time for each measurement was only 8 seconds, so this sensor array can be applied to repeated measurements. Figure 7(c) shows the evaluation result of temperature dependence of the fluorescent sensor. In the experiment, the initial temperature was set 37°C. The temperature was varied from 34°C to 40°C. In the fluorescence image of the sensor at each temperature, the fluorescence intensities of nine points were acquired, and the relative values of the fluorescent intensities at each temperature were plotted using 37°C as a reference. From the evaluation results, the variation of fluorescent intensity was within 1%. Moreover, the fluorescent intensity of the sensor was not affected by external disturbances such as changes in ion concentration since the sensor was separated from the solution by PDMS layer. Therefore, this sensor could be used for stable OCR measurement of single oocyte.

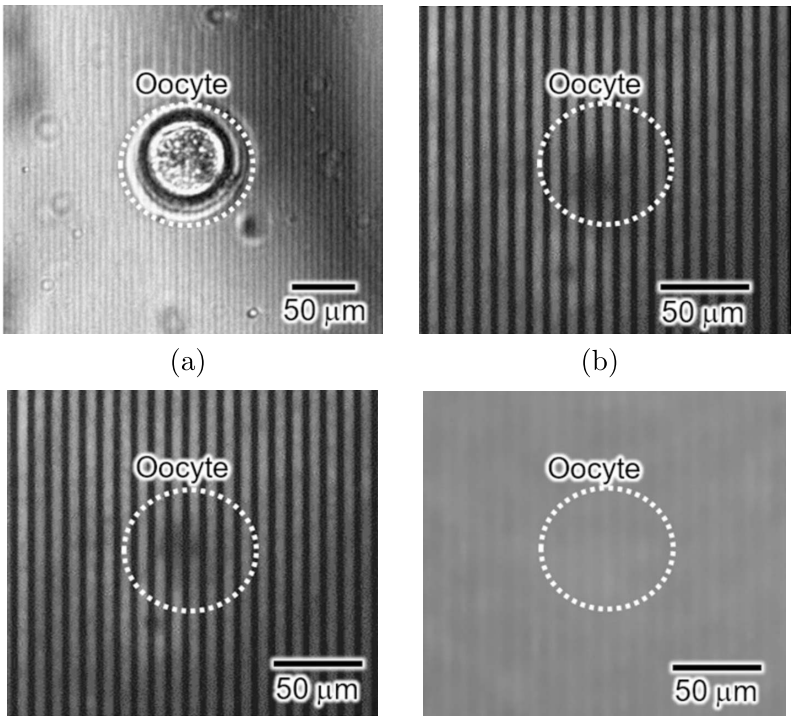


Figure 8: Measurement of OCR of single mouse oocyte using the fluorescent oxygen sensor. (a) A photograph of an oocyte, (b) Fluorescent image of the sensor without the oocyte, (c) Fluorescent image of the sensor with the oocyte. (d) Image of the fluorescent intensity ratio.

### 3.2. OCR measurement of a single oocyte

Figure 8 shows the result of OCR measurement of single mouse oocyte using the fluorescent sensor. The size of the mouse oocyte was 120 $\mu$m. The temperature was kept at 37°C and the $CO_2$ concentration at 5%. The exposure time for acquiring fluorescence images was set to 8 seconds. First, a reference fluorescent image was acquired with no oocyte. The oocyte was then placed on the microchamber (white dot circle). Five minutes after the oocyte was placed, the fluorescent image with the oocyte was acquired. From the information on fluorescent intensity in Figure 8(b) and Figure 8(c), an image of fluorescent intensity ratio was obtained as shown in Figure 8(d). The oxygen concentration distribution was calculated by Figure 8(d) and

equation 5. Figure 9 (a) and Figure 9 (b) show the bright-field image of the measured oocyte (sample 1) and the two-dimensional profile of the measured oxygen concentration, respectively. In Figure 9(b), data in the place without the sensors are plotted the linearly interpolated data on the sensors. Figure 9 (c) shows the oxygen concentration profile in 4 directions. The oxygen concentration profile was calculated for four directions using oxygen concentration distribution data and equation 5. The direction of A is upper left 45°, that of B is lower left 45°, that of C is upper right 45°, that of D is lower right 45°. Each dot in the graph represented the fluorescence intensity of the oxygen sensor. Because pixel size in the fluorescence image is 1 $\mu$m and the width or gap of the sensor is 5 $\mu$m, each of the five dots was shown intermittently. From Figure 9 (c), oxygen concentration profile $C(r)$ was fitted by equation 6.

$$C(r) = \alpha + \frac{\beta}{r} \tag{6}$$

In direction A, the values of $\alpha$ and $\beta$ were determined to be 142 and $-1.6843 \times 10^{-8}$ respectively by the least-squares method. Then, the slope of the oxygen concentration profile at the oocyte surface was determined by equation 7.

$$\left(\frac{dC(r)}{dr}\right)_{r=r_s} = \left(-\frac{\beta}{r^2}\right)_{r=r_s} \tag{7}$$

From equations 4, 7, and $\alpha$ ($= -1.6843 \times 10^{-8}$) and $r_s$ ($= 60\mu$m), the OCR in direction A was calculated 0.58 fmol/s. Moreover, the average value of OCR of sample 1 in four directions (A, B, C, D) was 0.59 fmol/s. OCR measurements were also performed on the other five oocytes. All oocytes were represented as a two-dimensional profile with oxygen concentration increasing circumferentially from the oocyte surface, as shown in Figure 9(b). The trend was the same for all oocytes, even though the magnitude of the slope of the profiles differed. Table 2 shows the calculated values of OCR in each direction for six mouse oocytes. The averaged OCR of six oocytes was 0.31 fmol/s. In this paper, frozen primary oocytes were used. The variation of OCR is considered the effect of oocyte damaged by freezing and thawing procedure, and individual difference of oocytes. From previous report, the OCR of the primary mouse oocyte was approximately 0.38 fmol/s [21]. OCR values between the measurement results and the previous report were considered comparable. These results indicate that we have successfully measured the two-dimensional OCR of a single oocyte on a microchamber.

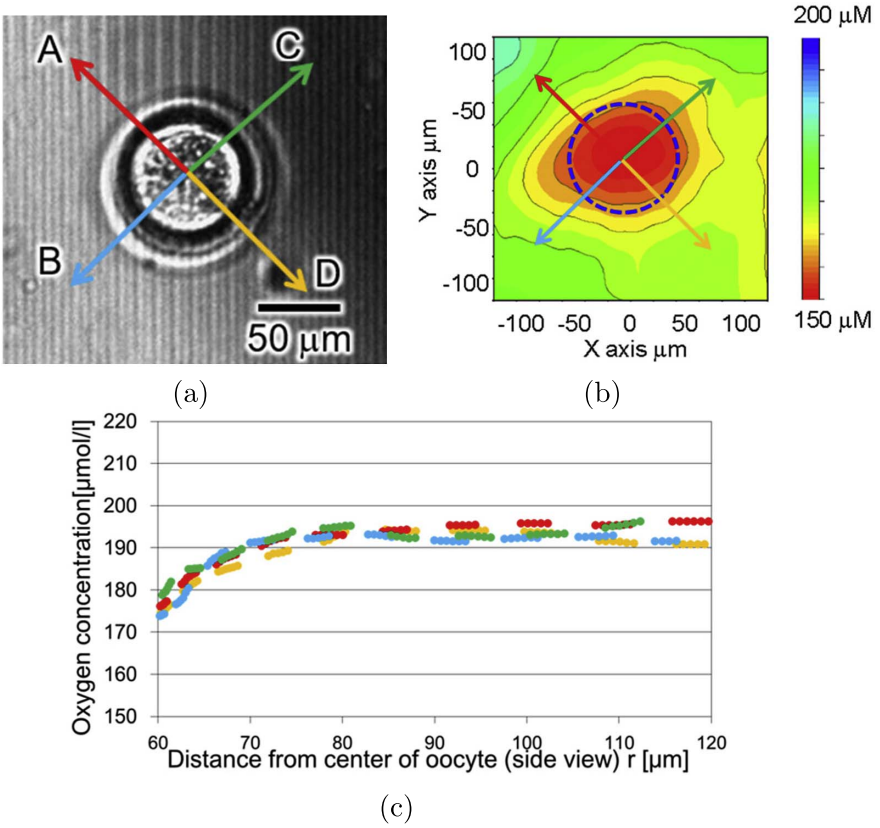


Figure 9: Measurement result of oxygen profile. (a) The direction of OCR measurement, (b) The Color map of oxygen concentration, (c) Profile of oxygen concentration ($r_s = 60\mu$m). The white circle indicates the area in which the oocyte exists.

## 4. Conclusions

This paper reported a non-contact method for OCR measurement of single oocytes by a fluorescent sensor array. The fluorescent sensor was composed of PEGDA 575 and an oxygen-sensitive fluorescent indicator, $Ru(bpy)_3Cl_2$. The sensor was designed with a stripe pattern in the PDMS microchannel to prevent contacting the fluorescent material with the oocyte, so that the OCR could be calculated using the spherical diffusion theory. This method allowed us to measure the OCR of a single oocyte in any direction on the microchamber in a non-contact manner. With this method, the OCR distri-

Table 2: OCR distribution in single oocytes

| No. | OCR [fmol/s] | | | | Average of OCR [fmol/s] | Divergence of OCR [fmol/s] |
|---|---|---|---|---|---|---|
| | A | B | C | D | | |
| 1 | 0.58 | 0.56 | 0.60 | 0.64 | 0.59 | 0.03 |
| 2 | 0.53 | 0.23 | 0.66 | 0.48 | 0.47 | 0.18 |
| 3 | 0.21 | 0.34 | 0.31 | 0.39 | 0.31 | 0.07 |
| 4 | 0.07 | 0.29 | 0.22 | 0.11 | 0.19 | 0.10 |
| 5 | 0.15 | 0.11 | 0.17 | 0.27 | 0.17 | 0.07 |
| 6 | 0.12 | 0.12 | 0.15 | 0.15 | 0.13 | 0.02 |

bution in two dimensions was calculated. Finally, rapid OCR measurement of the mouse oocyte, taking only 8 seconds for each measurement, was succeeded. This technique is expected to contribute the measurement of cell characteristics in various biomedical applications.

## References

[1] P. V-Juncá, I. Irarrázaval, A. J. Rolle, J. I. Gutiérrez, R. D. Moreno, Manuel J. Santos, *In vitro fertilization (IVF) in mammals: epigenetic and developmental alterations. Scientific and bioethical implications for IVF in humans*. Biological Research, **48**:68(13 pages), 2015.

[2] T. Ishikawa, T.Kyoya, Y.Nakamura, Eimei Sato,T. Tomiyama, K. Kyono, *Oxygen consumption rate of early pre-antral follicles from vitrified human ovarian cortical tissue*. Journal of Reproduction and Development, **60**: 460–467, 2014.

[3] D.B. Papkovsky, R.I. Dmitriev, *Biological detection by optical oxygen sensing*. Chem. Soc. Rev., **19**(4):8700–8732, 2013.

[4] E. C-Fernandez, H. M. Picton, R. Dumollard, *Metabolism throughout follicle and oocyte development in mammals*. Int. J. Dev. Biol., **56**:799–808, 2012.

[5] L. Gu, H. Liu, X. Gu, C. Boots, K. H. Moley, Q. Wang, *Metabolic control of oocyte development: linking maternal nutrition and reproductive outcomes*. Cell. Mol. Life Sci., **72**:251–271, 2015.

[6] F. E. Duncan, S. Jasti, A. Paulson, J. M. Kelsh, B. Fegley, J. L. Gerton, C. Magnusson, T. Hillensjö, A. Tsafriri, R. Hurtborn, K. Aheren, *Age-associated dysregulation of protein metabolism in the mammalian oocyte*. Aging Cell, **16**:1381–1393, 2017.

[7] G. D Catandi, Y. M Obeidat, C. D Broeckling, T. W Chen, A. J Chicco, E. M Carnevale, *Equine maternal aging affects oocyte lipid content, metabolic function and developmental potential*. Nature, **493**:632–637, 2013.

[8] H. S. Ban, B.-K. Kim, H. Lee, H. M. Kim, D. Harmalkar, M. Nam, S.-K. Park, K. Lee, J.-T. Park, I. Kim, K. Lee, G.-S. Hwang, M. Won, *The novel hypoxia-inducible factor-1α inhibitor IDF-11774 regulates cancer metabolism, thereby suppressing tumor growth*. Cell Death and Disease, **8**:e2843(8 pages), 2017.

[9] D. Li, X. Na, W. Zhou, C. Wang, Y. Li, B.-W. Zhu, M. Tan, *Adverse effects of fluorescent carbon dots from canned yellow croaker on cellular respiration and glycolysis*. Food & Function, **10**:1123–1131, 2019.

[10] C. Corbet, E. Bastien, N. Draoui, B. Doix, L. Mignion, B. F. Jordan, A. Marchand, J.-C. Vanherck, P. Chaltin, O. Schakman, H. M. Becker, O. Riant, O. Feron, *Interruption of lactate uptake by inhibiting mitochondrial pyruvate transport unravels direct antitumor and radiosensitizing effects*. Nature Communication, **9**:1208(11 pages), 2018.

[11] T. Kuno, M. Tachibana, A. F.-Sato, M. Fue, K. Higashi, A. Takahashi, H. Kurosawa, K. Nishio, N. Shiga, Z. Watanabe, N. Yaegashi, *A Preclinical Evaluation towards the Clinical Application of Oxygen Consumption Measurement by CERMs by a Mouse Chimera Model*. Int. J. Mol. Sci., **20**:5650(16 pages), 2019.

[12] N. Morimoto, S. Hashimoto, M. Yamanaka, T. Nakano, M. Satoh, Y. Nakaoka, H. Iwata, A. Fukui, Y. Morimoto, H. Shibahara, *Mitochondrial oxygen consumption rate of human embryos declines with maternal age*. Journal of Assisted Reproduction and Genetics, **37**:1815–1821, 2020.

[13] C. S. Santos, F. Macedo, A. J. Kowaltowski, M. Bertotti, P. R. Unwin, F. M. da Cunha, G. N. Meloni, *Unveiling the contribution of the reproductive system of individual Caenorhabditis elegans on oxygen consumption by single-point scanning electrochemical microscopy measurements*. Analytica Chimica Acta, **1146**:88–97, 2021.

[14] H. Maruyama, T. Otake, F. Arai, *Photoprocessible hydrogel microsensor for local environment measurement on a microfluidic chip*. Transact. Mechatron., **15**:845–852, 2011.

[15] K. Komori, S. Fujii, K. Montagne, *Development of well-of-the-well*

*system-based embryo culture plate with an oxygen sensing photoluminescent probe*. Sensor. Actuat. B-Chem., **162**:278–283, 2012.

[16] K. Mizukami, A. Katano, S. Shiozaki, T. Yoshihara, N. Goda, S. Tobita, *In vivo O2 imaging in hepatic tissues by phosphorescence lifetime imaging microscopy using Ir(III) complexes as intracellular probes*. Scientific Reports, **10**:21053(14 pages), 2020.

[17] H. Maruyama, F. Arai, T. Fukuda, *On-chip pH measurement using functionalized gel-microbeads positioned by optical tweezers*. Lab Chip, **8**:346–351, 2008.

[18] H. Hashim, H. Maruyama, Y. Akita, F. Arai, *Hydrogel Fluorescence Microsensor with Fluorescence Recovery for Prolonged Stable Temperature Measurements*. Sensors, **19**:5247(13 pages), 2019.

[19] S. Richard, A. P. Tartia, D. Boison, J. M. Baltz, *Mouse Oocytes Acquire Mechanisms That Permit Independent Cell Volume Regulation at the End of Oogenesis*. Journal of Cellular Physiology, **232**:2436–2446, 2017.

[20] H. Kurosawa, H. Utsunomiya, N. Shiga, A. Takahashi, M. Ihara, M. Ishibashi, M. Nishimoto, Z. Watanabe, H. Abe, J. Kumagai, Y. Terada, H. Igarashi, T. Takahashi, A. Fukui, R. Suganuma, M. Tachibana, N. Yaegashi, *Development of a new clinically applicable device for embryo evaluation which measures embryo oxygen consumption*. Human Reproduction, **31**:2321–2330, 2016.

[21] S. E Harris, H. J Leese, R. G Gosden, H. M Picton, *Pyruvate and oxygen consumption throughout the growth and development of murine oocytes*. Molecular Reproduction & Development, **76**:231–238, 2009.

Hisataka Maruyama
Department of Micro-Nano Systems Engineering
Nagoya University
Furo-cho, Chikusa-ku
Nagoya, Aichi, 464-8603, Japan
*E-mail address:* hisataka.maruyama@mae.nagoya-u.ac.jp

Fumihito Arai
Department of Mechanical Engineering
The University of Tokyo
7-3-1 Hongo, Bunkyo-ku
Tokyo 113-8656, Japan
*E-mail address:* arai-fumihito@g.ecc.u-tokyo.ac.jp

Received March 25, 2021